Calcium speciation and coordination environment in intracellular amorphous calcium carbonate (ACC) formed by cyanobacteria

Neha Mehta, Delphine Vantelon, Juliette Gaëtan, Alejandro Fernandez-Martinez, Ludovic Delbes, Cynthia Travert, Karim Benzerara

Calcium speciation and coordination environment in intracellular amorphous calcium carbonate (ACC) formed by cyanobacteria

Neha Mehta[1], Delphine Vantelon[2], Juliette Gaëtan[1], Alejandro Fernandez-Martinez[3], Ludovic Delbes[1], Cynthia Travert[1], Karim Benzerara[1]*

[1]Sorbonne Université, Muséum National d'Histoire Naturelle, UMR CNRS 7590. Institut de Minéralogie, de Physique des Matériaux et de Cosmochimie (IMPMC), 4 Place Jussieu, 75005 Paris, France.

[2]Synchrotron SOLEIL, L'Orme des Merisiers, Départementale 128, 91190 Saint-Aubin, France

[3]Université Grenoble Alpes, Université Savoie Mont Blanc, CNRS, IRD, IFSTTAR, ISTerre, F-38000 Grenoble, France.

*Corresponding author: karim.benzerara@sorbonne-universite.fr

Keywords: biomineralization; cyanobacteria; amorphous calcium carbonate; XANES; EXAFS; Ca K-edge

Abstract

An increasing number of bacteria has been shown to form intracellular amorphous calcium carbonates (ACC), as previously observed for biomineralizing eukaryotes. Yet, the short-range order of these bacterial intracellular ACC remains largely unexplored. Because ACC in bacteria is easily lost upon sample preparation, the use of *in situ* techniques is required to probe ACC within intact cells at the atomic scale. Here, we show the application of X-ray absorption near-edge structure (XANES) and extended X-ray absorption fine structure (EXAFS) spectroscopies to study the calcium (Ca) speciation and coordination environment in intact cells of diverse ACC-forming cyanobacteria. Our results show that XANES was effective in detecting ACC in intact cells. Between 60-85% of the total Ca in ACC-forming cyanobacteria strains is contained in the ACC phase and the rest in a single phase or a mixture of amorphous phases, possibly Ca complexed by organic molecules. Moreover, the short-range order of cyanobacterial ACC was different from eukaryotic ACC. This short-range order was similar to monohydrocalcite. These findings shed light on the fate of cyanobacterial ACC and the role of ACC-forming cyanobacteria in the Ca biogeochemical cycle.

1. Introduction:

Amorphous calcium carbonate (ACC) is a common precursor of carbonate eukaryotic biominerals (e.g. [1–4]). The formation of such a precursor may be instrumental in the control of the ultimate morphology, structure, and trace element chemical composition of the biomineralized structures formed by organisms ([5–7]). In its pure form, ACC is a soluble and reactive precipitate and is generally accepted as relatively unstable under physiological conditions [1]. How organisms control the formation, stability, and transformation of ACC remains a long-standing question in the field of biomineralization [8–10]. Recent studies have shown that ACC is also widespread in bacteria [9,11,12]. These bacteria are found in diverse environments including sediments, marine, freshwater, and brackish water [11,13,14]. The repertoire of ACC-forming bacteria includes at least 21 strains of cyanobacteria affiliated to diverse genera [14,15], one sulfur-oxidizing gammaproteobacterium affiliated to *Achromatium*, and a group of bacteria called magnetotactic bacteria (MTB) affiliated to Alphaproteobacteria and Gammaproteobacteria [8,9]. Using comparative genomics, Benzerara et al. proposed that ACC formation by cyanobacteria is a genetically controlled process, involving a new gene family [14]. The formation of ACC within bacteria can occur even when the extracellular medium is undersaturated, suggesting that ACC formation costs energy to the cells, presumably in relation to the active sequestration of Ca [16]. Balancing this cost, multiple roles have been proposed for ACC in bacteria including an intracellular pH buffer, or a storage form of calcium (Ca) and/or carbon (C) [17]. Moreover, the ACC inclusions formed by some cyanobacteria strains sequester high concentrations of alkaline earth elements such as Ba, Sr, or Ra, including the radioactive isotopes (^{90}Sr and ^{226}Ra), which holds two implications: 1) these cyanobacteria may be overlooked actors in the biogeochemical cycles of these trace elements[18,19]; (2) they may offer some potential for remediating pollutions by these radioactive isotopes [20,21].

While pure abiogenic ACC is highly unstable, transforming within minutes to crystalline calcium carbonate ($CaCO_3$) polymorphs such as calcite, or aragonite, ACC found in bacteria remains stable intracellularly with no obvious spontaneous transformation to crystalline phases such as calcite [22]. This behavior is similar to stable biogenic ACC found in eukaryotes that remain stable intracellularly [23]. While eukaryotes are known to form metastable biogenic ACC (aka transient biogenic ACC), which acts as a precursor phase for the formation of calcite and aragonite minerals in skeletal architectures[1–4,24–26], this metastability has not been observed yet in prokaryotes. Various organic or inorganic additives (Mg, P), structural water, and/or confinement of ACC within small volumes, have been proposed to promote the stabilization of biogenic ACC [27–31]. Confinement may be one of the stabilizing mechanisms in cyanobacteria since Blondeau et al. showed that cyanobacterial ACC granules are contained within an envelope of undetermined biochemical composition, either a lipid monolayer and/or proteins [32].

Despite the widespread occurrence of ACC-forming bacteria and their biogeochemical significance, little is known about the short-range structure of bacterial ACC. To date, our knowledge of the short-range structure of ACC is derived from experimental work on eukaryotic ACC. These studies show that biogenic and synthetic ACC have a distinct short-range order with proto-structures resembling different crystalline calcium carbonate ($CaCO_3$) phases. For example, ACC in aragonitic freshwater snail *Biomphalaria glabrata* was found to have a short-range order similar to aragonite [33]. Short-range orderings close to that of aragonite and calcite were found in aragonitic larval mollusks and calcitic sea urchin structures, respectively[1,34,35]. Monohydrocalcite-like ACC has also been reported in a series of other organisms [23]. This observation gave rise to the widely accepted notion that polyamorphism exists in biogenic ACC [1,36]. These differences in short-range order are attributed to the organisms producing ACC and thus might be genetically controlled

(e.g. [1,4,28,37,38]). Although these studies have brought a novel perspective to our understanding of biomineralization processes and nucleation pathways, there is a lack of structural studies on ACC found in different types of bacteria.

This study aims to address this knowledge gap by characterizing the local structure of ACC found in bacteria. This is not a trivial task because ACC in bacteria is easily lost upon sample preparation, and therefore its study requires the use of *in situ* techniques that could probe ACC within intact cells at the atomic scale [21,39]. One such tool for the study of relatively disordered mineral phases is X-ray absorption spectroscopy (XAS), comprising X-ray near-edge structure (XANES) and extended X-ray absorption fine structure (EXAFS) spectroscopies. XANES is particularly suited for chemical speciation studies of elements [40] and has been widely used to study eukaryotic ACC (e.g. [23,41,42]). EXAFS is another powerful tool to study amorphous precipitates such as ACC which lacks long-range order and provides complementary information to depict the coordination symmetry, bond distances, and the nature and number of the nearest neighboring atoms around Ca at high spatial resolution. Several studies have used EXAFS at the Ca K-edge to study the short-range order of biogenic ACC extracted from eukaryotes and synthetic ACC with a focus to understand biomineralization and nucleation pathways (e.g.[35,42,43]). Accordingly, the objectives of the present study are (1) to test the ability of Ca K-edge XANES to detect ACC within intact cells of bacteria; (2) to characterize the local order of bacterial ACC using EXAFS and to compare it with the reported structure of eukaryotic ACC. The ACC-forming cyanobacteria strains were selected here as model systems for this study because (1) they are the only ACC-forming bacteria that can be cultured in the laboratory; (2) they are phylogenetically and environmentally diverse, allowing the study of the influence of different biological factors on intracellular ACC formation [14].

2. Materials and method

2.1. Abiotic Ca-bearing reference phases

Six powdered reference Ca-bearing mineral phases were studied: calcite ($CaCO_3$), calcium pyrophosphate ($Ca_2P_2O_7$), hydroxyapatite ($Ca_{10}(PO_4)_6(OH)_2$), (all purchased from Sigma Aldrich ™) and naturally occurring aragonite ($CaCO_3$) (sample from the mineral collection at Sorbonne University, Paris, France). These references were selected to represent the type of phases expected to be found in environments of interest and/or associated with cyanobacteria.

Moreover, since some cyanobacterial ACC contain magnesium (Mg)[e.g. 39], a series of amorphous calcium-magnesium carbonates (referred to as ACC) samples were synthesized to examine variations in the Ca K-edge XANES spectra of ACC as a function of their Mg content[44–46]. They are labeled as ACC1 to ACC8 and syn ACC and their synthesis conditions are listed in Table S1. Samples were precipitated by mixing two solutions at concentrations listed in Table S1: (i) an aqueous carbonate solution containing K_2CO_3 (for syn ACC) or Na_2CO_3 (for ACC1–8) (pH = 11.4); and (ii) an aqueous calcium and magnesium solution containing $CaCl_2.2H_2O$ (Sigma-Aldrich) and $MgCl_2.6H_2O$ (adjusted to pH = 8.6). Ultra-pure water (MilliQ®) was used for all the preparations. All chemicals used were analytical grade. All solutions were prepared and kept in a fridge at 4°C for several hours prior to the synthesis. The calcium- and magnesium-containing solution was poured directly into the carbonate solution, under constant stirring. The resulting precipitate was isolated by centrifugation, washed twice with anhydrous ethanol, and dried either in a dry desiccator (for ACC1–8) or at 37°C for 7 days (syn ACC). The amorphous character of ACC1–8 and syn ACC was confirmed by quick X-ray diffraction (XRD) (data shown only for syn ACC), that showed only broad peaks (Figure S1). The Ca:Mg ratio of the ACC1–8 samples was determined using a Varian 720 ES ICP optical emission spectrometer (Geochemistry-Mineralogy

platform, ISTerre, Grenoble). A few milligrams of each sample were dissolved in 2% HNO_3 prior to the ICP measurements. For syn ACC, previous reports using the same synthesis protocols resulted in a Ca:Mg molar ratio of 2.5 [47]. Attenuated total reflectance Fourier transform infrared spectroscopy (ATR-FTIR) was performed on a selected synthetic ACC sample: syn ACC. For FTIR analysis: ATR-FTIR spectra were acquired over the mid-IR region (600-4000 cm^{-1}) using a NICOLET 6700 FT-IR spectrometer equipped with a diamond internal reflection element (IRE), a KBr beam splitter and a mercury cadmium telluride (MCT) detector. The dry synthetic ACC sample was mounted on the diamond IRE. Spectra were accumulated by collecting 64-100 scans at a resolution of 1 cm^{-1}. The FTIR spectrum of synthesized ACC showed the presence of a shoulder at 1474 cm^{-1} and the absence of a peak at 712 cm^{-1} (Figure S2), both of which are characteristic of ACC [48]. Synthesized ACC was stored at room temperature in a desiccator and remained amorphous for at least 1 year, as confirmed by XRD and FTIR spectroscopy (data not shown).

2.2. Cyanobacteria cultures

Here, we refer to strains forming intracellular ACC as ACC (+) strains and strains not forming intracellular ACC as ACC (-) strains. We studied three ACC (-) strains and five ACC (+) strains. These strains were *Synechocystis* sp. PCC 6803 (ACC-), *Microcystis* sp. PMC 568 (ACC-), *Microcystis* sp. PMC 810 (ACC-), *Cyanothece* sp. PCC 7425 (ACC+), *Synechococcus* sp. PCC 6312 (ACC+), *Microcystis* sp. PMC 827 (ACC+), *Microcystis* sp. PMC 831 (ACC+) and *Gloeomargarita ahousahtiae* (ACC+). All strains were cultured in a standard BG-11 medium[49]. Except the *Microcystis* strains (PMC 569, PMC 810, PMC 827, PMC 831), and *G. ahousahtiae*, the rest of the strains were cultured under continuous agitation and continuous light (5-10 µmol m^{-2} s^{-1}). *G. ahousahtiae* was grown without agitation at 37 °C, under continuous light (5-10 µmol m^{-2} s^{-1})[50]. All *Microcystis* strains were grown without agitation, at 23 °C, with a 12:12 photoperiod

and a light intensity of ~ 5 µmol m^{-2} s^{-1}. The cell suspensions of all strains were harvested by centrifugation, rinsed, and dried at 40 °C for 48 hours. The presence/absence of ACC in these strains was assessed in a previous study by FTIR spectroscopy and electron microscopy [15,48]. Furthermore, X-ray diffraction patterns of all ACC (+) strains showed the absence of calcite and any other crystalline carbonates, consistently with previous studies documenting the amorphous nature of the intracellular carbonates by TEM and FTIR [e.g. 15,39,48,50] (Figure S3).

2.3 Ca K-edge XANES/EXAFS spectroscopy of biomass and abiotic Ca-bearing references

Dried biomass samples were diluted in cellulose and pressed into a 10 mm diameter pellet and mounted on Ca-free holders. XAS at the Ca K-edge was performed on the LUCIA beamline at the SOLEIL synchrotron (Saint-Aubin, France)[51,52]. The fixed exit double-crystal monochromator was equipped with Si (111) crystals. Spectra were recorded in the fluorescence mode for biomass samples using a 60 mm^2 mono-element silicon drift diode detector (Bruker), and in the transmission mode for Ca-bearing crystalline references and syn ACC using a silicon diode. The optimal amount of reference sample needed to prepare pellets for analysis in transmission mode was calculated using the X-ray absorption calculator XAFSmass (www.cells.es/Beamlines/CLAESS/software/xafsmass.html), to yield a theoretical edge jump of ~1. In the pre-edge region (3940-4030 eV), the spectra were collected with a step-size and a counting time of 2 eV and 1 s. The edge region (4030-4070 eV) was scanned with a step size and a counting time of 0.25 eV and 1 s. The EXAFS region (6270-6710 eV) was scanned with a step size increasing from 0.5 to 3 eV and a counting time from 1 to 3 s. Typically, 2-3 scans were acquired per sample in the fluorescence or transmission mode, which were then averaged. In some case, 5-7 scans were acquired to obtain a high signal-to-noise ratio in the EXAFS region. Each scan lasted for ~50 min. In both modes, the sample holder was positioned at 5° with respect to the fluorescence

188 detector to minimize self-absorption effects and maintained at a temperature of 77 K using a liquid
189 He-cryostat to minimize potential beam damages and localized heating. The energy was calibrated
190 using the calcite reference for which the first inflection point was set to 4045 eV.
191 Calcium K-edge XANES spectra of the ACC1–8 were collected on the "XAFS" beamline at
192 synchrotron Elettra (Trieste, Italy)[53]. Spectra were collected at the Ca K-edge (4038 eV) using a
193 Si (111) monochromator, in the transmission mode at a temperature of 100 K. Samples were
194 prepared in the form of pellets, diluted with graphite powder. Spectra were collected using the
195 current in two ionization chambers placed before and after the sample. Samples of calcite, a
196 nanocalcite, a Mg-calcite, dolomite and aragonite were measured at synchrotron Elettra as standards
197 (data not shown).

198 **2.4 XANES/EXAFS data analysis**

199 All XANES data were processed with the Athena software [54] using the Autbk algorithm (Rbkb =
200 1, k-weight = 3). Since the Ca K-edge XANES dataset of series of ACC1–8 and syn ACC were
201 acquired on different beamlines, they were aligned in energy using syn ACC as the reference prior
202 to normalizing the spectra. Normalized Ca-K edge spectra were obtained by fitting the pre-edge
203 region with a linear function and the post-edge region with a quadratic polynomial function. The
204 angle to the detector and the Ca concentration in the samples were low enough to prevent self-
205 absorption effect, thus they were not corrected. The Ca K-edge XANES spectra of the reference
206 samples reported in this study were collected in the transmission mode. The XANES derivative
207 spectra of ACC+ cyanobacteria strains were analyzed by linear combination fitting (LCF), available
208 in the Athena software, in the 4028-4068 eV range; all components' weights were forced to be
209 positive. The LCF of Ca K-edge XANES derivative spectra of ACC (+) cyanobacteria strains was
210 performed using two endmembers: 1) a synthetic ACC representing Ca speciation in ACC; different

synthetic ACC with varying Ca: Mg ratio were used as a reference for synthetic ACC. (2) An ACC (-) cyanobacteria strain, corresponding to Ca in the non-ACC "matrix" present in cyanobacteria. The Ca speciation in ACC (-) cyanobacteria possibly corresponds to species such as Ca complexed by organics and/or Ca hosted by polyphosphate inclusions [55]. *Synechocystis* PCC 6803 (ACC-) was used as a reference fit component for strains *Cyanothece* 7425 (ACC+), *G. ahousahtiae* (ACC+), and *Synechococcus* 6312 (ACC+). *Microcystis* PMC 810 (ACC-) was used as a reference fit component for strains *Microcystis* PMC 831 (ACC+) and *Microcystis* PMC 827 (ACC+). We note that the fit of all *Microcystis* (ACC+) strains remained unaffected when *Microcystis* PMC 568 (ACC-) was used as a reference fit component instead of *Microcystis* PMC 810 (ACC-) (Table S2).

The Fourier transform of the k^3-weighted EXAFS spectra was calculated over the range of 2.8-10 $Å^{-1}$ using a Hanning apodization window (dk = 1). The EXAFS data were fitted in the 1.3–4.0 Å distance range with the ARTEMIS interface to IFEFFIT (Ravel and Newville, 2005) using least-squares refinements. Paths used for fitting were calculated from the aragonite structure[56] using the FEFF6 algorithm included in the ARTEMIS interface. The fit parameters were derived by fitting the EXAFS spectrum of the calcite reference. The corresponding fit is shown in Figure S4.

3. Results and Discussion

3.1. XANES spectra of synthetic ACC and cyanobacterial strains

The Ca K-edge XANES spectra were acquired for a series of synthetic ACCs that were synthesized with varying Ca: Mg molar ratios ranging between 0.8 to 8.6 (Table S1). No differences were observed in the Ca K-edge XANES spectra of the synthetic ACCs (Figure S5). Thus, for simplicity, hereafter, we refer to one representative synthetic ACC only (syn ACC) that contained

a Ca: Mg molar ratio of 2.5 [47]. The Ca K-edge normalized absorption and derivative spectra of a syn ACC and abiotic Ca-bearing reference phases (calcite, aragonite, hydroxyapatite, and calcium pyrophosphates) are shown in Figure 1A-B. Several features are observed in the XANES spectrum of syn ACC that distinguish it from other Ca-bearing reference compounds. First, the XANES spectrum of syn ACC has a pronounced pre-edge feature A_1 at 4040.46 eV (1s→3d type transition), which is absent in calcite and more discrete in aragonite (Figure 1A). This may indicate a deviation of ACC structure from centrosymmetric structures like those of calcite and aragonite [57] [58]. Second, the B_1 feature in the derivative XANES spectrum of syn ACC at 4043.41 eV (1s→ 4p type transition[59]), was weak, whereas it was pronounced in calcite, aragonite, hydroxyapatite, and calcium pyrophosphate (Figure 1B). Moreover, the position of B_1 at 4043.41 eV, as seen in the derivative XANES spectrum of syn ACC, was shifted compared with other phases such as calcite (ΔE= -0.16 eV), aragonite (ΔE= -0.48 eV), hydroxyapatite (ΔE= 0.89 eV), calcium pyrophosphate (ΔE= 1.14 eV) (Figure S6), suggesting that the position of the B_1 feature at 4043.41 eV was a characteristic feature of ACC. This may result from a difference in the symmetry of the environment around the Ca atom in syn ACC as compared with the references used here [60]. Third, the derivative XANES spectrum of syn ACC has a feature C_1 at 4045.41 eV (1s→ 4p transition[61]), which is absent in hydroxyapatite and calcium pyrophosphate, and sharper and pronounced in calcite and aragonite (Figure 1B). Moreover, the position of C_1 at 4045.41 eV, as seen in the derivative of the XANES spectrum of syn ACC, was shifted compared with that of calcite (ΔE= -0.85 eV) and aragonite (ΔE= -0.32) eV. Lastly, the syn ACC shows a single broad peak D_1 at the absorption edge at ~4048 eV without the splitting seen in calcite and hydroxyapatite or any pronounced features seen at energies greater than 4050 eV for aragonite, calcite, and hydroxyapatite (Figure 1A). The differences in spectral features (i.e. A_1, B_1, C_1, D_1 in Figure 1A-B) between syn ACC and other Ca-

bearing phases are consistent with previous studies showing that XANES at Ca K-edge is efficient in discriminating between ACC and crystalline Ca-carbonate phases and other Ca-containing phases (e.g. [58,60–63]). Below we discuss how these spectral characteristics appear when comparing Ca K-edge XANES spectra of intact cells of ACC-forming cyanobacteria strains (referred to hereafter as ACC (+) strains), and intact cells of cyanobacteria strains not forming ACC (referred to as ACC (-) strains).

Figure 1C shows normalized Ca K-edge XANES spectra for ACC (+) (#1 to #5) and ACC (-) (#6 to #8) cyanobacteria strains along with reference syn ACC. All the strains irrespective of ACC forming capability had a pre-edge feature A_2 at 4040 eV and an absorption edge D_2 at 4048.45 eV. These XANES features matched that of syn ACC perfectly well (A_1 at 4040 eV and D_1 at 4048.45 eV). Moreover, the presence of a pre-edge feature (A_2) and a broad absorption edge (D_2) in the XANES spectra of all the strains confirms the absence of calcite (Figure 1A and Figure 1C). No additional XANES features were observed in the spectra of all cyanobacteria strains, also suggesting the absence of any additional crystalline Ca-bearing phase. In contrast, notable differences were observed upon comparing the derivative XANES spectra ACC (+) and ACC (-) cyanobacteria strains. While all cyanobacteria strains (ACC (+) and ACC (-)) had a feature in their derivative XANES spectra at 4045.02 eV (labeled as C_2) that coincides with the C_1 feature observed in syn ACC, only ACC (+) cyanobacteria strains (#1-5) had a clear feature at 4043.41 eV, labeled as B_2 in the derivative XANES spectra, that coincides with the characteristic position of the B_1 feature in the derivative XANES spectrum of syn ACC (Figure 1D). The energy positions of the B_1 and C_1 features in the derivative of the XANES spectrum of syn ACC were effective for discriminating syn ACC from calcite. However, in biogenic ACC, the C_1 feature was also present in the ACC (-) cyanobacteria strains, and therefore the C_1 feature was not effective in discriminating

Ca environments present in both ACC (+) and ACC (-) strains. Thus, the only spectral feature discriminating between the Ca environments in ACC (+) and ACC (-) strains was the B_1 feature. As B_1 is characteristic of ACC (see previous discussion), its presence in ACC (+) cyanobacteria and absence in ACC (-) cyanobacteria strains makes it a marker of ACC in cells. Overall, the present experimental approach and methodology were able to detect ACC in intact cells of different cyanobacterial strains. Furthermore, except for the position of the B_1 feature, other characteristic spectral features of ACC (i.e. A_1, C_1, D_1) were not effective in discriminating between the Ca environment found in ACC (+) and ACC (-) cyanobacteria strains.

Interestingly, the B_1 feature was also reported in the ACC of body spicules but not in the ACC from the lobster carapace and plant cystoliths [23]. However, we note that we used derivative XANES spectra to clearly detect the B_1 feature in ACC (+) cyanobacteria, whereas no derivative spectra of the different eukaryotic ACC were examined by the previous studies to the best of our knowledge. Overall, this may have led to missed detection of the weak B_1 feature of ACC in lobster carapace and plant cystolith. Alternatively, the inconsistency between the XANES spectral features observed in eukaryotic ACC and cyanobacteria ACC could be simply due to the fact that they are different from one another. For example, they have different chemical compositions: ACC in plant cystolith has 26 atoms % magnesium (Mg) and no phosphorus (P); ACC in spicules of *Pyura pachydermatina* has 0-16 atom % Mg and up to 55 atom % P; ACC in lobster carapace has 12-20 atom % Mg, and 33-49 atom % P, whereas ACC in cyanobacteria contains less than 3 atom % Mg and up to 1.7 atom % P [18,23] (Table S3). However, several observations suggest that the variation in the Mg and P content of ACC was not correlated with the presence or absence of the B_1 feature. First, despite comparable P contents of ACC in spicules of *Pyura pachydermatina* and ACC in the lobster carapace, the B_1 feature was only detected in the ACC in spicules. Furthermore, syn ACC

had 25 atoms % of Mg and still showed the presence of the B_1 feature in its XANES spectrum. Last, the XANES Ca K-edge spectra collected on the series of synthetic ACC with varying Ca: Mg content all showed the B_1 feature (Figure S5). Biogenic ACC is also known to contain organic additives as stabilizing agents [64,65]. Whether variations in organic content of biogenic ACC could possibly be linked with the presence or absence of B_1 feature remains unknown. Indeed, in the derivative Ca K-edge XANES spectra of Ca complexed with different organic ligands such as oxalate, humus, and acetate, the B_1 feature was not found [66]. However, due to the paucity of reliable quantitative data about the organic content of different biogenic ACC (eukaryotic and bacterial), further exploration of the role of organic additives on appearance of B_1 feature remains limited for the moment, but an interesting topic for future studies. Nevertheless, the perfect match of the spectral features of syn ACC and ACC (+) cyanobacteria strains, the absence of crystalline carbonates signatures in XANES spectrum of ACC (+) cyanobacteria strains, the presence of the B_1 feature in ACC (+) cyanobacteria strains at an energy position that coincides with the characteristic B_1 feature of syn ACC and its absence in ACC (-) cyanobacteria strains, altogether confirm that 1) XANES was effective in detecting ACC in intact cells of cyanobacteria, and the sample preparation method did not induce any ACC crystallization that could be detected by XANES (or by XRD), and 2) the energy position of feature B_1 in derivative XANES spectrum of syn ACC is a promising diagnostic indicator of ACC presence in the cyanobacteria strains. The feature is weak and can be readily overlooked from a cursory examination of XANES spectra or potentially in ACC associated with higher proportions of organics. The generalization of the B_1 feature as a universal indicator of eukaryotic and prokaryotic ACC remains to be seen in future studies, but based on our results, this feature appears as a reliable diagnostic of ACC in cyanobacteria.

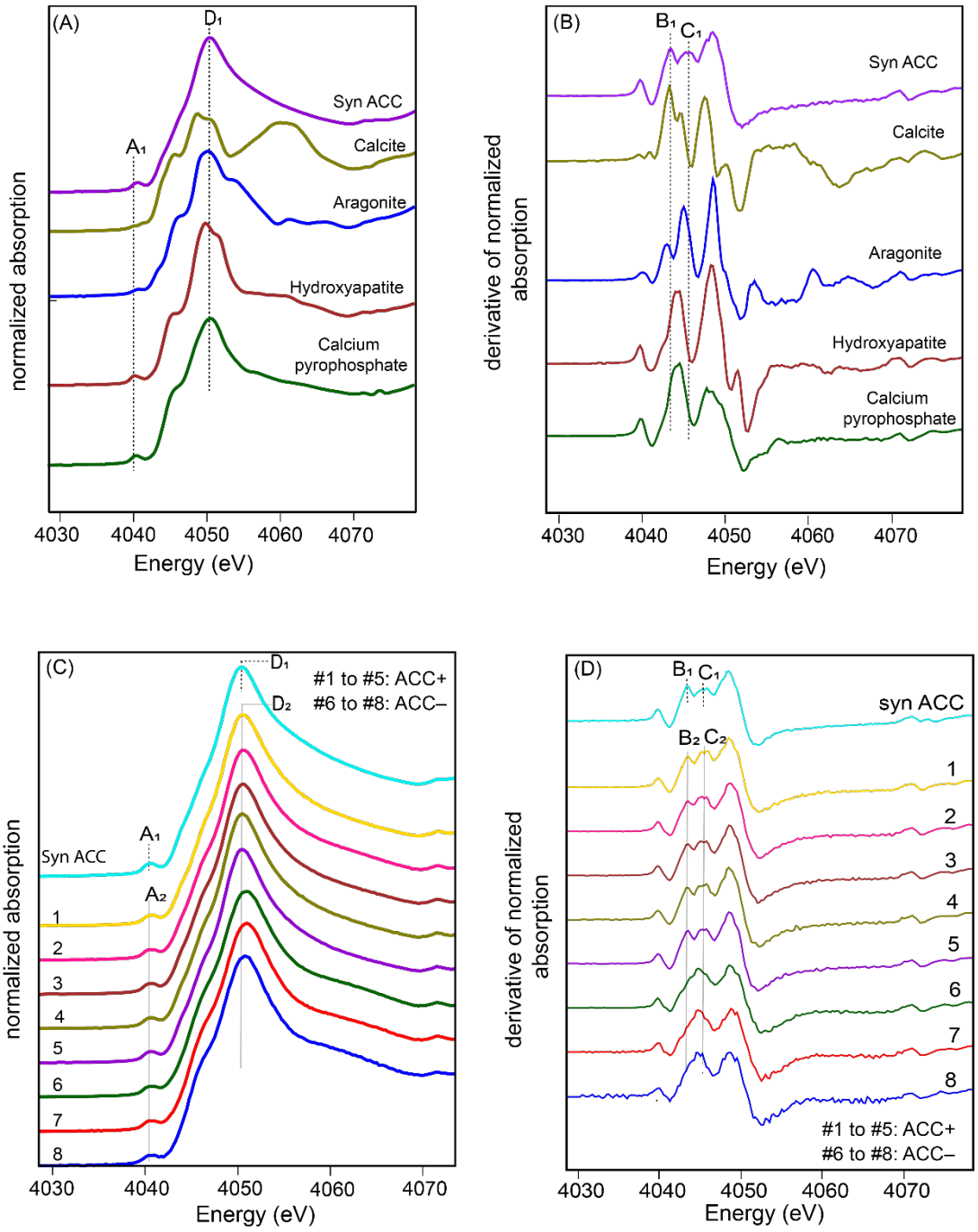

Figure 1: (A) Normalized XANES spectra of syn ACC and other abiotic Ca-bearing reference compounds. (B) derivate XANES spectra of syn ACC and other abiotic Ca-bearing reference compounds. (C) Normalized Ca-K edge and (D) derivate XANES spectra of ACC (+) and ACC (-) cyanobacteria strains as denoted by #1-8: (1) *G. ahousahtiae* (ACC+), (2) *Microcystis* PMC 831 (ACC+), (3) *Microcystis* PMC 827 (ACC+), (4) *Synechococcus* PCC 6312 (ACC+), (5) *Cyanothece* PCC 7425 (ACC+), (6) *Microcystis* PMC 568 (ACC-), (7) *Microcystis* PMC 810 (ACC-), (8) *Synechocystis* PCC 6803 (ACC-). Synthetic ACC spectra (syn ACC) shown for reference. The dashed lines indicate the position of spectral features A_1, B_1, C_1 and D_1 in XANES and derivates XANES spectrum of syn ACC. The solid grey lines indicate the position of A_2, B_2, C_2, D_2 in XANES and derivates XANES spectra of ACC (+) cyanobacteria strains (See text for details).

We used linear combination fitting (LCF) to quantify the proportion of different Ca reservoirs in ACC (+) cyanobacteria strains. These spectra were fitted under the assumption that there are two different environments for Ca in ACC (+) cyanobacteria strains: 1) intracellular ACC and 2) a non-ACC matrix that represents all Ca contained inside/at the surface of the cells in a form different from ACC (e.g., Ca complexed by organics; Ca associated with polyphosphates). Based on this fit, it is then possible to assess the proportion of Ca contained within ACC over the total Ca cell reservoir. Detailed LCF fit analyses are provided in section 2. The fit results are shown in Figure 2 and Table S2. Depending on the strain, the proportion of Ca in ACC to total Ca in ACC (+) cyanobacteria ranged from 60-84%, with an error on the weight of each component assessed to ~ 10% (Figure 2B). The variation in the proportion of Ca in ACC to total Ca in ACC (+) cyanobacteria strains is consistent with the previous studies estimating ACC content in ACC (+) cyanobacteria strains and suggesting a variable ACC content between strains [48]. The exact reasons underlying the differences in the proportion of Ca in ACC across strains remain unknown. Some hypothesis includes differences in the use and function of Ca in ACC among strains, and variations in cellular Ca demand among strains. Nevertheless, our results confirm that ACC is the largest reservoir of Ca in ACC-forming cyanobacteria. These findings are relevant when considering the role of ACC-forming bacteria in the Ca biogeochemical cycle. To date, the documented occurrence of ACC-forming bacteria in the environment is often mixed with other Ca-containing phases such as crystalline calcium carbonates or Ca-P-containing phases, especially when the extracellular fluid is oversaturated with respect to these phases [67]. Such co-occurrence makes it challenging to quantify the relative importance of ACC-forming bacteria compared to other Ca-bearing phases. Our proposed methodology could be an effective tool to address this challenge as this approach

351 quantifies Ca phases at a bulk scale and unambiguously discriminates between amorphous *vs*
352 crystalline Ca-containing carbonates and Ca-P bearing phases.
353

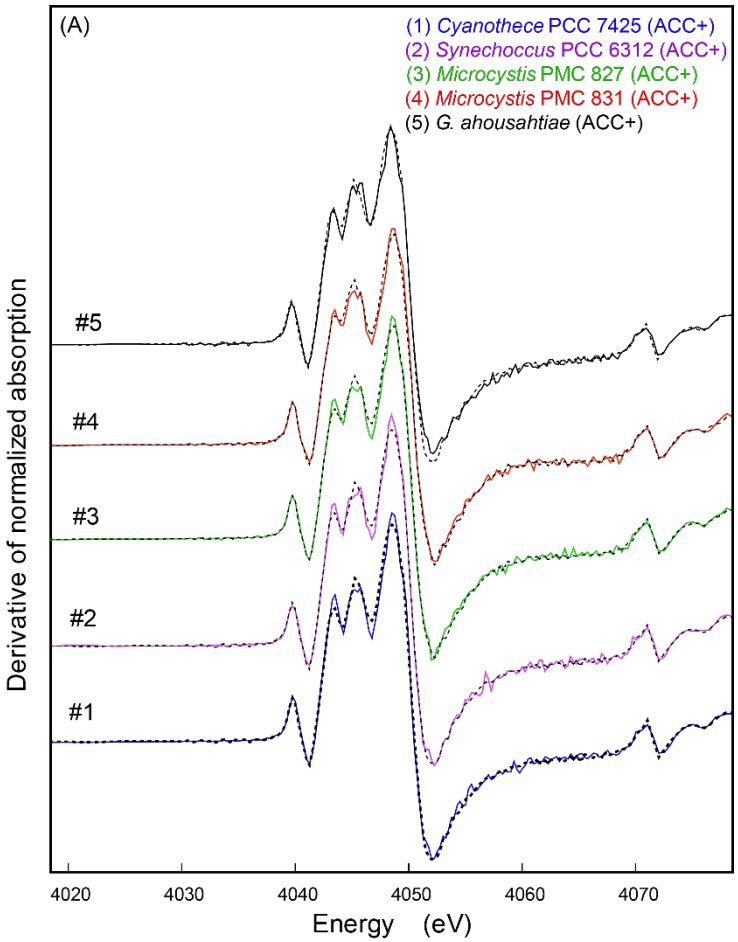

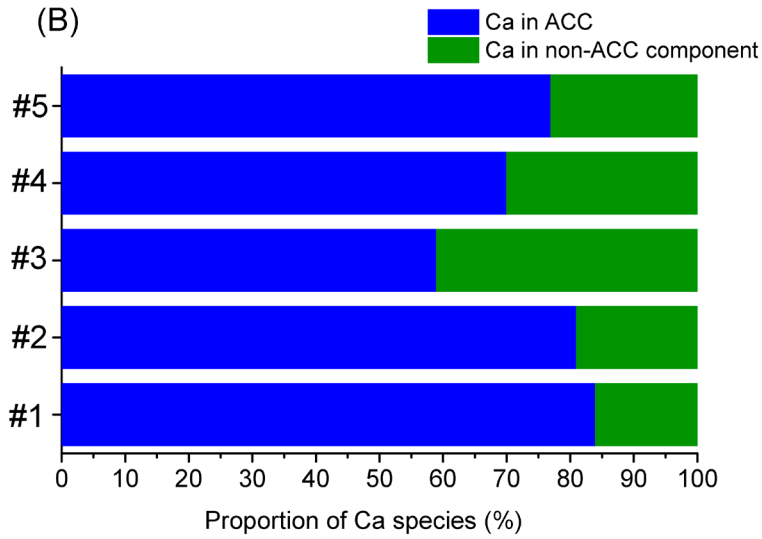

Figure 2: (A) Ca-K edge spectra of ACC (+) strains. Solid lines are experimental data and dotted lines are the LCF results. (B): Proportion of ACC and ACC (-) strain to Ca speciation in ACC (+) strains determined by LCF of the XANES data shown in Fig. 1. The error on the weight of each component if ~10%.

3.2. Local order of cyanobacterial ACC

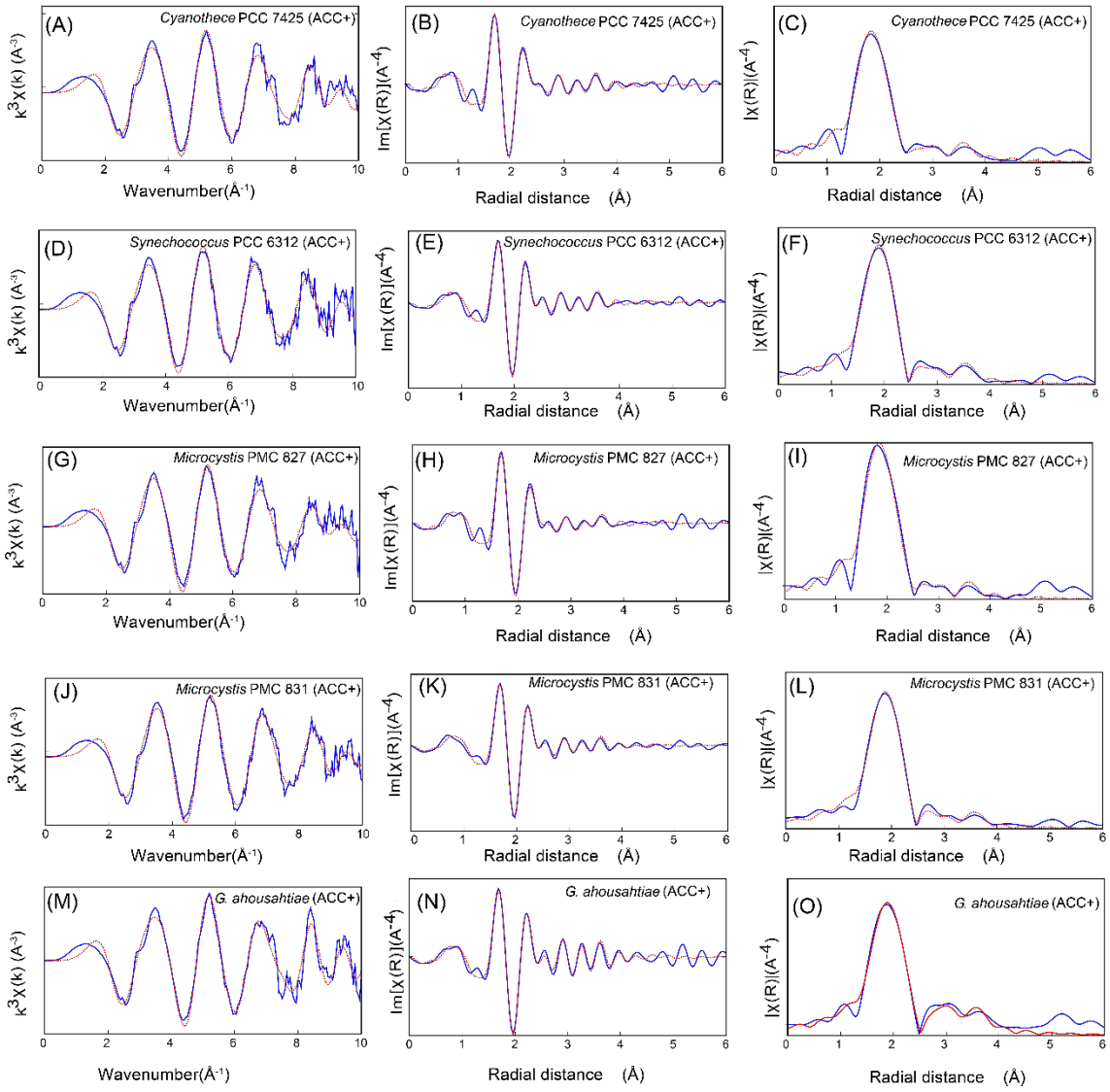

Figure 3: Ca K-edge EXAFS spectra ($k^3[\chi(k)]$; A, D, G, J, M), imaginary part (B, E, H, K, N) and Fourier transformed magnitudes (C, F, I, L, O) of Ca in *Cyanothece* PCC 7425 (ACC+), *Synechococcus* PCC 6312 (ACC+), *Microcystis* PMC 827 (ACC+), *Microcystis* PMC 831 (ACC+), and *G. ahousahtiae* (ACC+). The data is in solid blue lines and model fits are shown as red dotted lines. The EXAFS data were fitted in the 1.3–4.0 Å distance range. The fitted values of coordination number, radial distance, and associated Debye-Weller factors for each shell are summarized in Table 1. The amplitude reduction factors S_0^2 and ΔE_o were respectively set to 0.88 and 0.41 eV.

Table 1: Coordination number, radial distance and associated Debye-Weller factors obtained by fits for each shell for all ACC (+) strains. The amplitude reduction factor S_0^2 and ΔE_o were respectively set to 0.88 and 0.41 eV; N is the coordination number of the scatterer in the shell, and *R* is the bond distance between the scatterers (Ca, C, O) and Ca. The Debye-Weller factors for each shell were fixed.

	Ca-O			**Ca-O**			**Ca-C**			**Ca-Ca**			**R-factor**
	N	**R (A°)**	**σ^2**	**N**	**R (A°)**	**σ^2**	**N**	**R (A°)**	**σ^2**	**N**	**R (A°)**	**σ^2**	
Cyanothece PCC 7425 (ACC+)	4.3 ± 0.2	2.35 ± 0.01	0.002	3.8 ± 0.2	2.52 ± 0.01	0.002	3.3 ± 0.7	3.41 ± 0.02	0.002	0.6 ± 0.2	3.89 ± 0.02	0.002	0.0113
Synechococcus PCC 6312 (ACC+)	3.8 ± 0.2	2.35 ± 0.01	0.002	3.8 ± 0.2	2.49 ± 0.01	0.002	3.0 ± 0.7	3.56 ± 0.02	0.002	0.7 ± 0.2	3.86 ± 0.02	0.002	0.0083
Microcystis PMC 827 (ACC+)	4.1 ± 0.2	2.34 ± 0.01	0.002	4.1 ± 0.2	2.50 ± 0.01	0.002	2.6 ± 0.7	3.57 ± 0.02	0.002	0.5 ± 0.2	3.86 ± 0.02	0.002	0.0167
Microcystis PMC 831 (ACC+)	3.7 ± 0.2	2.33 ± 0.01	0.002	4.0 ± 0.2	2.48 ± 0.01	0.002	2.5 ± 0.7	3.57 ± 0.02	0.002	0.6 ± 0.2	3.87 ± 0.02	0.002	0.0059
G. ahousahtiae (ACC+)	3.8 ± 0.2	2.34 ± 0.01	0.002	4.1 ± 0.2	2.49 ± 0.01	0.002	4.4 ± 0.7	3.57 ± 0.02	0.002	0.7 ± 0.2	3.90 ± 0.02	0.002	0.0108

371 Table 2: EXAFS fitting of the Ca K-edge spectra of (i) the cyanobacterial ACC (this study) and (ii) representative eukaryotic ACC and
372 crystalline $CaCO_3$ samples (all parameters extracted from the literature, see references indicated for each line). *CN* is the coordination
373 number, and *R* is the bond distance between the scatterer and Ca.

	Ca-O			***Ca-C***			***Ca-Ca***		
	CN	R	σ^2 (Å^2)	CN	R	σ^2 (Å^2)	CN	R	σ^2 (Å^2)
ACC in cyanobacteria (this study)***	3.7-4.3 3.8-4.1	2.33-2.35 2.48-2.52	0.002 0.002	2.5-4.4	3.41-3.57	0.002	0.5-0.7	3.86-3.90	0.002
ACC in plant cystoliths *Ficus microcarpa* [23]***	2.3 3.3	2.22 2.42	0.005 0.0002	2*	3.5	0.040	4*	3.79	0.013
ACC in carapaces of *Homarus American* [23]***	1.9 3.9	2.23 2.41	0.005 0.003	4*	3.47	0.013	2*	3.79	0.013
ACC in spicules of *Pyura Pachyderma tina* [23]***	7.4	2.374	0.009	1.5 3	3.03 3.36	0.006 0.000			
ACC in sternal deposits of *Porcellio scaber* [42]**	3.8	2.38	0.014	1.4 0.4	3 3.72	0.007 0.001	6	3.89	0.109
ACC in larval shells of *Biomhalaria gabrata* [33]**	9	2.44	0.0309				6	3.92	0.047
Calcite [42]	6	2.33	0.009	6	3.27	0.035	6	4.05	0.009
Aragonite [42,60]	3 6	2.21 2.43	0.005 0.009	3 3	2.98 3.26	0.003 0.010	6	3.94	0.028
Monohydrocalcite [43]	8.2	2.42	0.014	4	3.04	0.022	2	3.83	0.005
Vaterite [60]	6	2.37	0.013				6	4.21	0.023

* fixed parameter during the fitting
** Transient biogenic ACC
*** Stable biogenic ACC

The Ca K-edge EXAFS spectra, imaginary part, and magnitude of Fourier transformed EXAFS of all ACC (+) strains along with the model fits and the best-fit parameters are shown in Figure 3 and Table 1. As a comparison, EXAFS spectra of ACC (-) strains are shown in Figure S7. The EXAFS spectra of ACC (+) strains were fitted using three shells of scatterers. Depending on the strain, the first coordination shell was fitted with a split shell of 7.6-8.2 oxygen (O) atoms in total, including 3.7-4.3 O atoms at 2.33-2.35 Å, and 3.8-4.1 O atoms at 2.48-2.52 Å. Strains *Synechococcus* PCC 6312, *G. ahousahtiae*, and *Microcystis* PMC 831 had a slightly lower number of O atoms in the first coordination shell relative to *Cyanothece* PCC 7425 and *Microcystis* PMC 827 (7.6-7.9 *versus* 8.1-8.2) (Table 1). The splitting of the Ca-O bond distance in cyanobacterial ACC was consistent with the results from previous studies on biogenic stable ACC as well as synthetic ACC [58]. The second coordination shell was fitted with 2.5-3.3 carbon (C) atoms at 3.41-3.57 Å for all strains but *G. ahousahtiae*, for which the second coordination was best fitted with 4.4 C atoms at 3.57 Å. The Ca-C bond distance in cyanobacterial ACC is similar to the monodentate linkages present in crystalline carbonates, suggesting that Ca and C associations in cyanobacterial ACC are predominantly monodentate [58]. Lastly, the third coordination shell was fitted with 0.5-0.7 Ca atoms at 3.86-3.90 Å. The addition of more shells did not improve the fit quality. While the Debye-Weller factor of 0.002 for the Ca-Ca shell is relatively small compared with that reported for biogenic ACC (0.047-0.109), re-fitting the Ca-Ca shell with a high Debye-Waller factor resulted in an increased R-factor of the EXAFS fit (Table S4). Therefore, we chose a lower Debye-Weller factor for a higher-order shell, which was kept fixed for all shells during the fit. Overall, the Ca coordination environment showed similarities across ACC (+) strains, with slight differences (e.g. Ca-C coordination shell) that could be reflective of polyamorphism within cyanobacterial ACC.

Upon comparing the Ca coordination environment between cyanobacterial ACC and non-cyanobacterial biogenic ACC, certain similarities and differences can be identified (Table 2). Broadly, the Ca-O and Ca-C coordination number (CN) and bond distances of cyanobacteria ACC are consistent with the ranges reported for other biogenic stable ACC phases (Table 2). Cyanobacterial ACC has the lowest number of Ca neighbors (0.5-0.7 Ca atoms) compared to other biogenic ACC (2-6 Ca atoms). Dilution of Ca-Ca coordination environment in cyanobacterial ACC by non-ACC components could result in low Ca CN. In this case, the number of Ca neighbors in ACC (+) cyanobacteria (0.5-0.7 Ca atoms) would reflect a weighted average between the Ca coordination numbers in ACC and non-ACC components. The dilution effect on Ca-Ca coordination environment can be corrected by assuming zero Ca neighbors in non-ACC components and deriving the proportion of Ca hosted in ACC *versus* non-ACC components from XANES data (60-84 % for ACC *versus* 40-16% for non-ACC). This results in an increase in the Ca-Ca bonds from 0.5-0.7 to 0.7-0.9. Considering the errors associated with the fits, the dilution-corrected Ca atoms in Ca-Ca is still among the lowest of the Ca coordination number measured among biogenic ACC. Such a dilution was likely minimized in other occurrences of biogenic ACC that had higher Ca CN, possibly because in these cases the ACC was separated from the organism (Table 2). In the case of bacterial ACC, isolation of ACC from the cells was not possible because it tends to dissolve and/or transform [21,39]. Alternatively, higher Debye-Weller sigma square (σ^2) values for the EXAFS fit of previously reported biogenic ACC (0.047-0.109) relative to cyanobacterial ACC (0.002) could also increase the Ca CN [23,33,68]. Last, a low Ca-Ca coordination number should be interpreted cautiously due to the large uncertainty associated with coordination number (20%).

418 Furthermore, the number of O atoms surrounding Ca in cyanobacterial ACC (7.6-8.2) is
419 closer to that in monohydrocalcite (MHC) (8.2 O atoms) than aragonite (9 O atoms), within an
420 uncertainty of 20% (Table 1). The number of Ca atoms in the fourth co-ordination shell in
421 cyanobacterial ACC (0.5-0.7 Ca atom) is also closer to MHC (2 Ca atom) than any other $CaCO_3$
422 crystalline polymorph, within an uncertainty of 20% (Table 1). The distance of the Ca–Ca shell is
423 significantly shorter at 3.86-3.90 Å in cyanobacterial ACC compared with calcite (4.06 Å), vaterite
424 (4.21 Å), and aragonite (3.99 Å), and closer to MHC (3.89 Å) (uncertainty 1%). These observations
425 suggest that the local order of cyanobacterial ACC encodes an MHC-like structure. Other
426 occurrences of biogenic stable ACC such as the body spicules of the ascidian *Pyura*
427 *pachydermatina*, ACC located in the carapace of the lobster *Homarus americanus*, and cystoliths
428 from the leaves of the plant *Ficus microcarpa* are also described as possessing short-range
429 structures resembling MHC [23]. Such a resemblance may indicate a stoichiometry of ACC similar
430 to that of MHC ($CaCO_3.H_2O$) [7,43,48]. No direct measurements of the water content of
431 cyanobacterial ACC were done. However, we note that cyanobacterial ACC is stable and that so
432 far all biogenic stable ACC occurrences are hydrated[10]. Indeed, the incorporation of water in ACC
433 has been linked to hampering the rearrangement of ions, thereby stabilizing ACC against
434 crystallization [69]. Second, water bands have been identified in cyanobacterial ACC FTIR
435 spectrum[48]. Overall, we conclude that the cyanobacterial ACC phase is most likely hydrated and
436 a stable ACC phase, and MHC is a suitable structural model for biogenic stable ACC not only in
437 eukaryotes but also in ACC-forming cyanobacteria.

438 The incipient structure encoded in biogenic ACC may be linked to the structure of the
439 final crystallization product of ACC, which is relevant when considering the fate of cyanobacterial
440 ACC in the extracellular environment, although this has not been studied yet. Under some

441 conditions, there seems to be a direct transformation of ACC to a crystalline carbonate that
442 involves dehydration of ACC and subsequent structural rearrangement of ACC to a crystalline
443 carbonate (e.g.[29,70,71]). Schmidt et al. showed that in synthetic ACC, dehydration proceeds without
444 significant changes in the immediate environment around the Ca ions, suggesting that the incipient
445 structure might remain preserved during ACC transformation [72,73]. Consistently, syntheses of
446 ACC in presence of aspartic acid showed short-range structures resembling vaterite, and upon
447 crystallization produced a mixture of vaterite and calcite and ultimately calcite[60]. Hasse et al.
448 suggested that ACC in the embryo of freshwater snail encoded an aragonite-like structure, which
449 later transformed into an aragonitic shell of the adult snail [33]. Based on the encoding of MHC-
450 like structure in cyanobacterial ACC, one possible hypothesis regarding the fate of cyanobacterial
451 ACC upon cell death could be that upon cell death cyanobacterial ACC may transforms to MHC
452 outside the cell, where MHC may dissolve or transform into other polymorphs of $CaCO_3$ or remain
453 stable[67]. Either of these outcomes will undoubtedly rely on the extracellular fluid chemistry of
454 environments hosting ACC-forming cyanobacteria.

455 While encoding of MHC in the local order of cyanobacterial ACC provides clues
456 regarding its extracellular stability and fate of cyanobacterial ACC in the environment, the
457 relationship between the intracellular stability of cyanobacterial ACC and local order is unclear.
458 One of the prevailing hypotheses for the stabilization of biogenic stable ACC suggests that the
459 creation of a unique microenvironment around ACC inhibits the formation of crystal nuclei,
460 thereby stabilizing ACC [1]. The creation of this environment is biologically controlled and
461 mediated through the action of biological macromolecules, and additives such as magnesium (Mg)
462 and phosphorus (P) [64]. The effect of these additives is not easily discernible in the local order of
463 biogenic stable ACC as evidenced by previous unsuccessful attempts to fit a Ca-Mg or Ca-P path

to the local structure of biogenic stable ACC and in this study as well (data not shown) [41]. These observations suggest that the concentrations of these additives are too low to be visible in EXAFS, indicating that if there is Mg or P contribution to the local order, it is not substantial. Similar conclusions were reached by Addadi et al[41]. Nevertheless, the presence of a distinct short-range order in cyanobacterial ACC is an indication of biological control on stabilizing ACC.

3. Conclusions

To summarize, this study presents a methodology using XANES and EXAFS at the Ca K-edge to study intracellular stable ACC in intact cells of cyanobacteria. Furthermore, our results provide valuable insights into the speciation of Ca in ACC-forming cyanobacteria strains using XANES LCF analysis. The results suggest that between 60-85% of the total calcium in ACC-forming cyanobacteria strains is contained in the ACC phase. Lastly, the Ca coordination environment of cyanobacterial ACC was different than other biogenic stable ACC, suggesting that cyanobacterial ACC is yet another type of ACC polymorph. The local order of cyanobacterial ACC was found to encode a structure similar to that of monohydrocalcite (MHC), similar to other biogenic stable ACC. How the cells impose this structure remains an interesting question for future work.

4. Acknowledgements

We would like to thank the financial support the French Agence Nationale de la Recherche (ANR), under grant ANR-19-CE44-0017-01. We thank Pierre Le Pape (IMPMC, Paris, France) for insightful discussions regarding interpretations of EXAFS spectra. We would also like to thank several instrumentation facilities located at L'Institut de Minéralogie, de Physique des Matériaux et de Cosmochimie (IMPMC, Paris, France) that enabled streamlines measurement and analysis of datasets presented in this work: Maxime Guillaumet and Keevin Béneut for Spectroscopy platform;

Ludovic Delbes and Benoît Baptiste for the X-ray diffraction facility; and Cynthia Travert and Feriel Skouri-Panet for GEMME (geomicrobiology) facility. We thank Cécile Bernard and Charlotte Duval from the Paris Museum collection (PMC) for providing PMC strains.

References

[1] B. L. Addadi, S. Raz, S. Weiner, *Adv. Mater.* **2003**, 959–970.
[2] I. M. Weiss, N. Tuross, L. Addadi, S. Weiner, *J. Exp. Zool.* **2002**, *293*, 478–491.
[3] Y. Politi, T. Arad, E. Klein, S. Weiner, L. Addadi, *Science.* **2004**, *306*, 1161–1164.
[4] J. Aizenberg, G. Lambert, S. Weiner, L. Addadi, *J. Am. Chem. Soc.* **2002**, *124*, 32–39.
[5] D. Evans, W. R. Gray, J. W. B. Rae, R. Greenop, P. B. Webb, K. Penkman, R. Kröger, N. Allison, *Geochim. Cosmochim. Acta* **2020**, *290*, 293–311.
[6] L. Gago-Duport, M. J. I. Briones, J. B. Rodríguez, B. Covelo, *J. Struct. Biol.* **2008**, *162*, 422–435.
[7] H. Du, E. Amstad, **2020**, 1798–1816.
[8] E. Couradeau, K. Benzerara, E. Gérard, D. Moreira, S. Bernard, G. E. Jr. Brown, P. López-García, *Science* **2012**, *336*, 459–462.
[9] K. Benzerara, F. Skouri-Panet, J. Li, C. Ferard, M. Gugger, T. Laurent, E. Couradeau, M. Ragon, J. Cosmidis, N. Menguy, I. Margaret-Oliver, R. Tavera, P. Lopez-Garcia, D. Moreira, *Proc. Natl. Acad. Sci.* **2014**, *111*, 10933–10938.
[10] S. Weiner, Y. Levi-Kalisman, S. Raz, L. Addadi, *Connect. Tissue Res.* **2003**, *44*, 214–218.
[11] C. L. Monteil, K. Benzerara, N. Menguy, C. C. Bidaud, E. Michot-Achdjian, R. Bolzoni, F. P. Mathon, M. Coutaud, B. Alonso, C. Garau, D. Jézéquel, E. Viollier, N. Ginet, M. Floriani, S. Swaraj, M. Sachse, V. Busigny, E. Duprat, F. Guyot, C. T. Lefevre, *ISME J.* **2021**, *15*, 1–18.
[12] K. Benzerara, R. Bolzoni, C. Monteil, O. Beyssac, O. Forni, B. Alonso, M. P. Asta, C. Lefevre, *Geobiology* **2021**, *19*, 199–213.
[13] M. Ragon, K. Benzerara, D. Moreira, R. Tavera, P. Lopez-Garcia, *Front. Microbiol.* **2014**, *5*, 1–11.
[14] K. Benzerara, E. Duprat, T. Bitard-Feildel, G. Caumes, C. Cassier-Chauvat, F. Chauvat, M. Dezi, S. I. Diop, G. Gaschignard, S. Görgen, M. Gugger, P. López-García, M. Millet, F. Skouri-Panet, D. Moreira, I. Callebaut, *Genome Biol. Evol.* **2022**, *14*, 1–16.
[15] J. Gaëtan, S. Halary, M. Millet, C. Bernard, C. Duval, S. Hamlaoui, A. Hecquet, M. Gugger, B. Marie, N. Mehta, D. Moreira, F. Skouri-Panet, C. Travert, E. Duprat, J. Leloup, K. Benzerara, *Environ. Microbiol.* **2022**, 1462-2920.16322.
[16] N. Cam, K. Benzerara, T. Georgelin, M. Jaber, J. F. Lambert, M. Poinsot, F. Skouri-Panet, D. Moreira, P. López-García, E. Raimbault, L. Cordier, D. Jézéquel, *Geobiology* **2018**, *16*, 49–61.
[17] J. Cosmidis, K. Benzerara, *Comptes Rendus Géoscience Planète* **2022**, *34*, 1–39.
[18] N. Cam, K. Benzerara, T. Georgelin, M. Jaber, J. F. Lambert, M. Poinsot, F. Skouri-Panet, L. Cordier, *Environ. Sci. Technol.* **2016**, *50*, 11654–11662.
[19] M. Blondeau, K. Benzerara, C. Ferard, J. M. Guigner, M. Poinsot, M. Coutaud, M. Tharaud, L. Cordier, F. Skouri-Panet, *Chem. Geol.* **2018**, *483*, 88–97.
[20] N. Mehta, K. Benzerara, B. D. Kocar, V. Chapon, *Environ. Sci. Technol.* **2019**, *53*, 12639–12647.
[21] N. Mehta, J. Bougoure, B. D. Kocar, E. Duprat, K. Benzerara, *ACS EST Water* **2022**, *2*, 616–623.
[22] M. E. Hodson, L. G. Benning, B. Demarchi, K. E. H. Penkman, J. D. Rodriguez-Blanco, P. F. Schofield, E. A. A. Versteegh, *Geochem. Trans.* **2015**, *16*, DOI 10.1186/s12932-015-0019-z.

[23] Y. Levi-Kalisman, S. Raz, S. Weiner, L. Addadi, I. Sagi, *Adv. Funct. Mater.* **2002**, *12*, 43–48.
[24] Y. Politi, R. A. Metzler, M. Abrecht, B. Gilbert, F. H. Wilt, I. Sagi, L. Addadi, S. Weiner, P. U. P. A. Gilbert, *Proc. Natl. Acad. Sci.* **2008**, *105*, 17362–17366.
[25] Y. Politi, Y. Levi-Kalisman, S. Raz, F. Wilt, L. Addadi, S. Weiner, I. Sagi, *Adv. Funct. Mater.* **2006**, *16*, 1289–1298.
[26] P. U. P. A. Gilbert, K. D. Bergmann, N. Boekelheide, S. Tambutté, T. Mass, F. Marin, J. F. Adkins, J. Erez, B. Gilbert, **2022**, *9653*.
[27] C. J. Stephens, S. F. Ladden, F. C. Meldrum, H. K. Christenson, *Adv. Funct. Mater.* **2010**, *20*, n/a-n/a.
[28] E. Loste, R. M. Wilson, R. Seshadri, F. C. Meldrum, *J. Cryst. Growth* **2003**, *254*, 206–218.
[29] Z. Liu, Z. Zhang, Z. Wang, B. Jin, D. Li, J. Tao, R. Tang, J. J. de Yoreo, *Proc. Natl. Acad. Sci. U. S. A.* **2020**, *117*, 3397–3404.
[30] J. Cavanaugh, M. L. Whittaker, D. Joester, *Chem. Sci.* **2019**, 5039–5043.
[31] P. U. P. A. Gilbert, S. M. Porter, C. Y. Sun, S. Xiao, B. M. Gibson, N. Shenkar, A. H. Knoll, *Proc. Natl. Acad. Sci. U. S. A.* **2019**, *116*, 17659–17665.
[32] M. Blondeau, M. Sachse, C. Boulogne, C. Gillet, J.-M. Guigner, F. Skouri-Panet, M. Poinsot, C. Ferard, J. Miot, K. Benzerara, *Front. Microbiol.* **2018**, *9*, 1–14.
[33] B. Hasse, H. Ehrenberg, J. C. Marxen, W. Becker, M. Epple, *Chem. - Eur. J.* **2000**, *6*, 3679–3685.
[34] I. M. Weiss, N. Tuross, L. Addadi, S. Weiner, *J. Exp. Zool.* **2002**, *293*, 478–491.
[35] S. Raz, P. C. Hamilton, F. H. Wilt, S. Weiner, L. Addadi, *Adv. Funct. Mater.* **2003**, *13*, 480–486.
[36] J. H. E. Cartwright, A. G. Checa, J. D. Gale, D. Gebauer, C. I. Sainz-Díaz, *Angew. Chem. - Int. Ed.* **2012**, *51*, 11960–11970.
[37] S. Kababya, A. Gal, K. Kahil, S. Weiner, L. Addadi, A. Schmidt, *J. Am. Chem. Soc.* **2015**, *137*, 990–998.
[38] S. Weiner, L. Addadi, *Annu. Rev. Mater. Res.* **2011**, *41*, 21–40.
[39] J. Li, I. Margaret Oliver, N. Cam, T. Boudier, M. Blondeau, E. Leroy, J. Cosmidis, F. Skouri-Panet, J.-M. Guigner, C. Férard, M. Poinsot, D. Moreira, P. Lopez-Garcia, C. Cassier-Chauvat, F. Chauvat, K. Benzerara, *Minerals* **2016**, *6*, 10.
[40] F. Caballero-Briones, F. J. Espinosa-Faller, V. Rejón, F. Chalé, E. Hernández-Rodríguez, A. Zapata-Navarro, J. L. Peña, *J. Cereal Sci.* **2014**, *60*, 7–10.
[41] Y. Levi-Kalisman, S. W. Scfi Raz, L. Addadi, I. Sagi, *J. Chem. Soc. Dalton Trans.* **2000**, 3977–3982.
[42] A. Becker, U. Bismayer, M. Epple, H. Fabritius, B. Hasse, J. Shi, A. Ziegler, *J. Chem. Soc. Dalton Trans.* **2003**, *3*, 551–555.
[43] M. Neumann, M. Epple, *Eur. J. Inorg. Chem.* **2007**, 1953–1957.
[44] S. Von Euw, T. Azaïs, V. Manichev, G. Laurent, G. Pehau-Arnaudet, M. Rivers, N. Murali, D. J. Kelly, P. G. Falkowski, *J. Am. Chem. Soc.* **2020**, *142*, 12811–12825.
[45] N. Koga, Y. Nakagoe, H. Tanaka, *Thermochim. Acta* **1998**, *318*, 239–244.
[46] A. V. Radha, A. Fernandez-Martinez, Y. Hu, Y.-S. Jun, G. A. Waychunas, A. Navrotsky, *Geochim. Cosmochim. Acta* **2012**, *90*, 83–95.
[47] H. Nebel, M. Epple, *Z. Anorg. Allg. Chem.* **2008**, *634*, 1439–1443.
[48] N. Mehta, J. Gaëtan, P. Giura, T. Azaïs, K. Benzerara, *Spectrochim. Acta. A. Mol. Biomol. Spectrosc.* **2022**, *278*, 121262.
[49] R. Y. Stanier, J. Deruelles, R. Rippka, M. Herdman, J. B. Waterbury, *Microbiology* **1979**, *111*, 1–61.
[50] T. Bacchetta, P. López-García, A. Gutiérrez-Preciado, N. Mehta, F. Skouri-Panet, K. Benzerara, M. Ciobanu, N. Yubuki, R. Tavera, D. Moreira, *Eur. J. Phycol.* **2023**, *0*, 1–10.
[51] A.-M. Flank, G. Cauchon, P. Lagarde, S. Bac, M. Janousch, R. Wetter, J.-M. Dubuisson, M. Idir, F. Langlois, T. Moreno, D. Vantelon, *Nucl. Instrum. Methods Phys. Res. Sect. B Beam Interact. Mater. At.* **2006**, *246*, 269–274.
[52] D. Vantelon, N. Trcera, D. Roy, T. Moreno, D. Mailly, S. Guilet, E. Metchalkov, F. Delmotte, B. Lassalle, P. Lagarde, A.-M. Flank, *J. Synchrotron Radiat.* **2016**, *23*, 635–640.

[53] G. Aquilanti, M. Giorgetti, R. Dominko, L. Stievano, I. Arčon, N. Novello, L. Olivi, *J. Phys. Appl. Phys.* **2017**, *50*, 074001.
[54] B. Ravel, M. Newville, in *J. Synchrotron Radiat.*, **2005**, pp. 537–541.
[55] B. Karim, G. Sigrid, K. M. Athar, C. Franck, M. Katia, M. Nicolas, M. Neha, S.-P. Fériel, S. Sufal, T. Cynthia, C.-C. Corinne, D. Elodie, *J. Electron Spectrosc. Relat. Phenom.* **2023**, *267*, 147369.
[56] J. P. R. De Villiers, *Am. Mineral.* **1971**, *56*, 758–767.
[57] A. Gaur, B. D. Shrivastava, *Rev. J. Chem.* **2015**, *5*, 361–398.
[58] J. Avaro, E. M. Moon, J. Rose, A. L. Rose, *Geochim. Cosmochim. Acta* **2019**, *259*, 344–357.
[59] J. L. Fulton, S. M. Heald, Y. S. Badyal, J. M. Simonson, *J. Phys. Chem. A* **2003**, *107*, 4688–4696.
[60] R. S. K. Lam, J. M. Charnock, A. Lennie, C. Fiona, R. S. K. Lam, J. M. Charnock, F. C. Meldrum, **2007**, DOI 10.1039/b710974a.
[61] F. M. Michel, J. MacDonald, J. Feng, B. L. Phillips, L. Ehm, C. Tarabrella, J. B. Parise, R. J. Reeder, *Chem. Mater.* **2008**, *20*, 4720–4728.
[62] L. Monico, L. Cartechini, F. Rosi, W. De Nolf, M. Cotte, R. Vivani, C. Maurich, C. Miliani, *Sci. Rep.* **2020**, *10*, 1–14.
[63] J. Xto, R. Wetter, C. N. Borca, C. Frieh, J. A. Van Bokhoven, T. Huthwelker, *RSC Adv.* **2019**, *9*, 34004–34010.
[64] D. Gebauer, H. Cölfen, A. Verch, M. Antonietti, *Adv. Mater.* **2009**, *21*, 435–439.
[65] M. Albéric, L. Bertinetti, Z. Zou, P. Fratzl, W. J. E. M. Habraken, Y. Politi, *Adv. Sci.* **2018**, *5*, 1701000–1701000.
[66] W. Li, X. Liu, Y. Hu, *Geostand. Geoanalytical Res.* **2020**, *44*, 805–819.
[67] N. Zeyen, K. Benzerara, O. Beyssac, D. Daval, E. Muller, C. Thomazo, R. Tavera, P. López-García, D. Moreira, E. Duprat, *Geochim. Cosmochim. Acta* **2021**, *305*, 148–184.
[68] A. Becker, U. Bismayer, M. Epple, H. Fabritius, B. Hasse, J. Shi, A. Ziegler, *Dalton Trans.* **2003**, 551–555.
[69] S. Sen, D. C. Kaseman, B. Colas, D. E. Jacob, S. M. Clark, *Phys. Chem. Chem. Phys.* **2016**, *18*, 20330–20337.
[70] A. Gal, W. Habraken, D. Gur, P. Fratzl, S. Weiner, L. Addadi, *Angew. Chem. Int. Ed.* **2013**, *52*, 4867–4870.
[71] Shuheng Zhang, O. Nahi, Li Chen, Zabeada Aslam, N. Kapur, Y.-Y. Kim, F. C. Meldrum, *Adv. Funct. Mater.* **2022**, 2201394–2201394.
[72] A. V. Radha, T. Z. Forbes, C. E. Killian, P. U. P. A. Gilbert, A. Navrotsky, *Proc. Natl. Acad. Sci. U. S. A.* **2010**, *107*, 16438–16443.
[73] M. P. Schmidt, A. J. Ilott, B. L. Phillips, R. J. Reeder, *Cryst. Growth Des.* **2014**, *14*, 938–951.

Supplementary information for

Calcium speciation and coordination environment in intracellular amorphous calcium carbonate (ACC) formed by cyanobacteria

Neha Mehta[1], Delphine Vantelon[2], Juliette Gaëtan[1], Alejandro Fernandez-Martinez[3], Karim Benzerara[1]*

[1]Sorbonne Université, Institut de Minéralogie, de Physique des Matériaux et de Cosmochimie (IMPMC), 4 Place Jussieu, 75005 Paris, France.

[2]Synchrotron SOLEIL, L'Orme des Merisiers, Saint-Aubin BP48, 91192 Gif-sur- Yvette Cedex, France

[3]Institut des Sciences de la Terre (ISTerre), Université de Grenoble 1, CNRS, 38041 Grenoble, France

*Corresponding author: karim.benzerara@sorbonne-universite.fr

Figure S1: Representative X-ray diffraction pattern of synthetic ACC's. XRD pattern was recorded between 2theta=3-70 degrees, with 0.001 degree steps and 2 milliseconds/step.

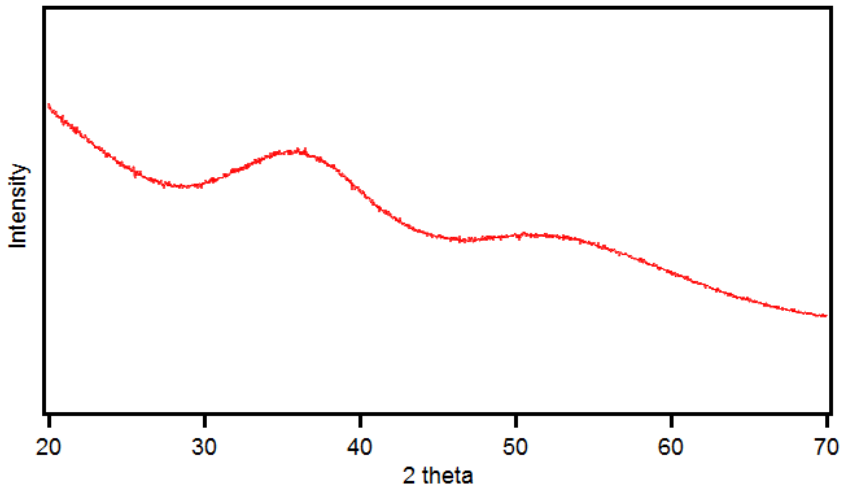

Figure S2: ATR-FTIR spectra of synthetic ACC in the mid-IR spectral range. The arrows correspond to characteristic mid-IR active frequencies of ACC.

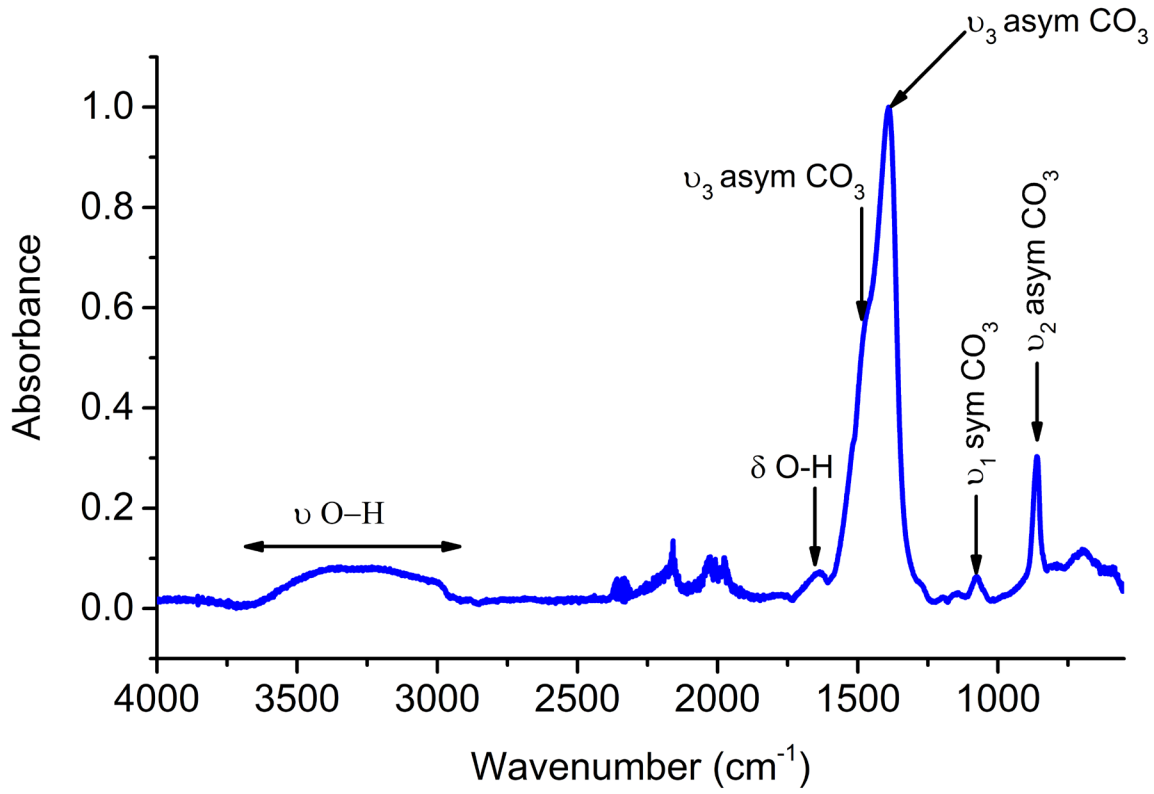

Figure S3: X-ray diffraction pattern of dried biomass pellets of ACC+ cyanobacteria strains mixed with cellulose (see main text, section 2.3). XRD pattern was recorded between 2theta=3-70°, with 0.001° steps and 2 milliseconds/step. The XRD pattern was recorded after acquiring Ca K-edge XANES spectra on the same sample. The peaks in XRD patterns of ACC+ cyanobacteria are due to presence of cellulose in the pellet (see reference diffractogram).

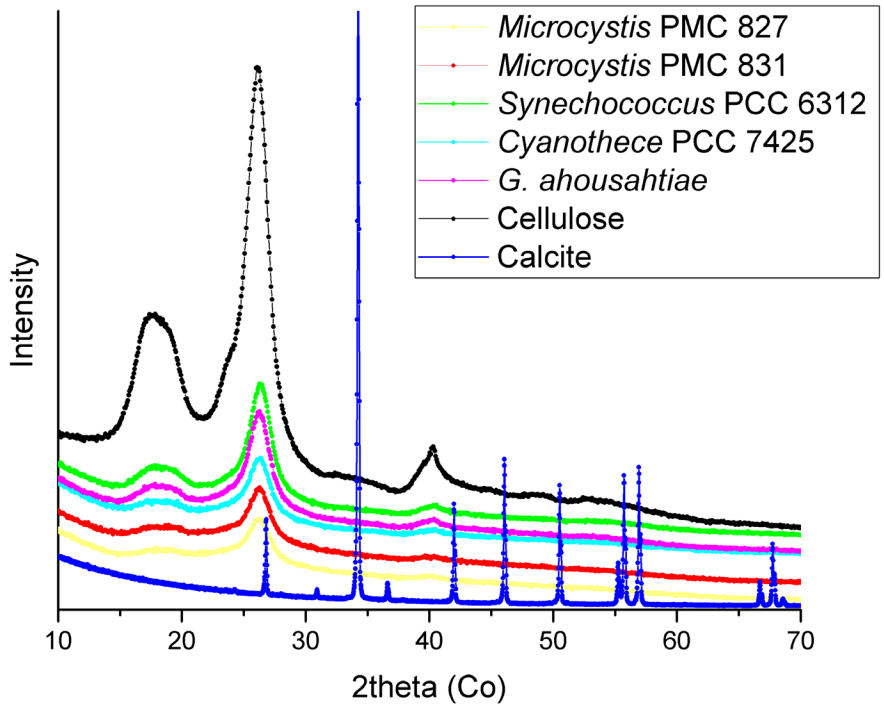

Figure S4: Ca K-edge EXAFS (blue) and back Fourier transform (purple) (Right), and magnitude and imaginary part (blue) of Fourier transformed spectrum (left) of calcite. The fit range is reported in green. The fit result is reported in red and light green for the back Fourier transform. The amplitude reduction factor S_0^2 and ΔE_o were set to 0.88 and 0.41 eV, respectively.

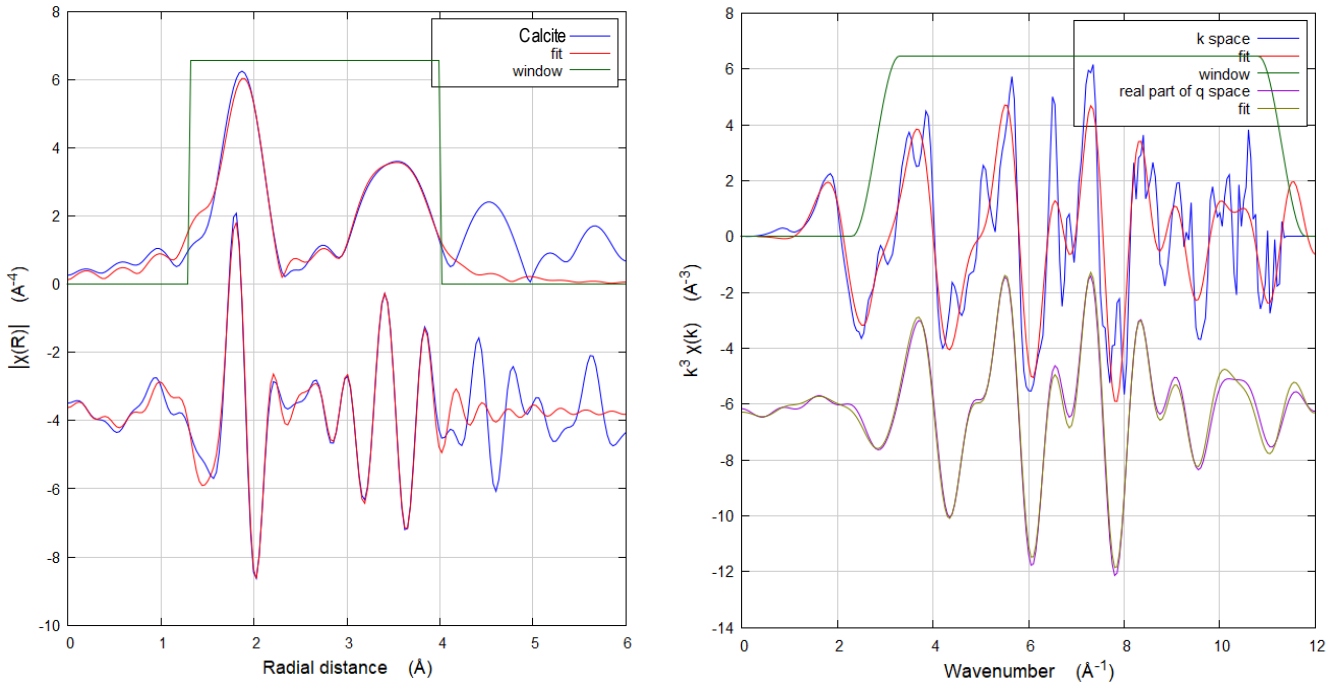

Figure S5: (A) Normalized Ca K-edge XANES spectra of and (B) derivative of the Ca K-edge XANES spectra of synthetic ACC with varying Ca: Mg molar ratio as listed in table S1. The dashed lines indicate the position of spectral features A_1, B_1, C_1 and D_1 in XANES and derivates XANES spectrum of synthetic ACCs'.

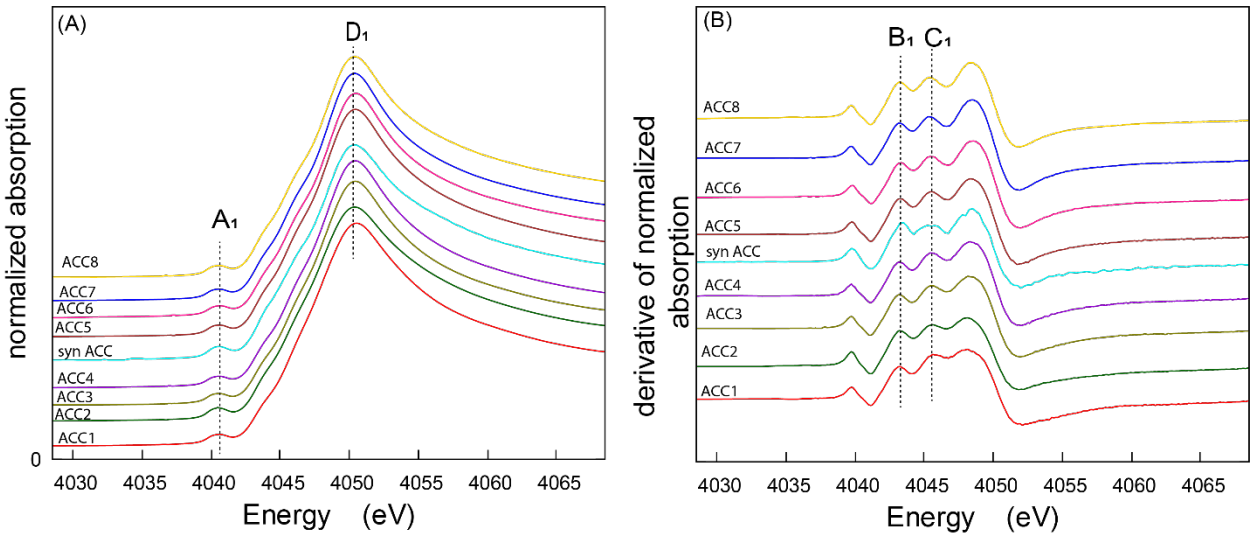

Figure S6: Derivative of the Ca K-edge XANES spectra of the references. The position of B_3 at 4043.41 eV, as seen in the derivative XANES spectrum of syn ACC, and marked by dashed line, was shifted compared with other phases: calcite (ΔE= -0.16 eV), aragonite (ΔE= -0.48 eV), hydroxyapatite (ΔE= 0.89 eV), calcium pyrophosphate (ΔE= 1.14 eV).

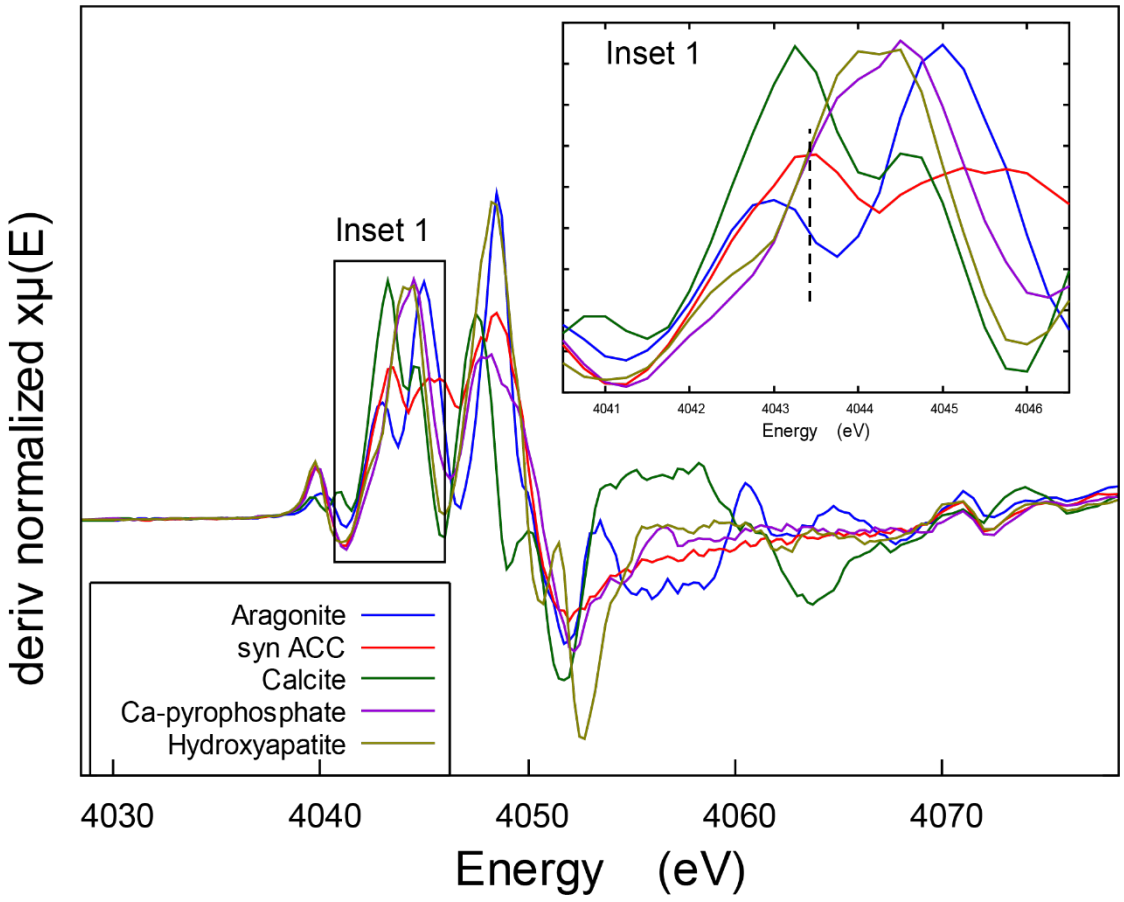

Figure S7: Ca K-edge EXAFS spectra ($k^3[\chi(k)]$) of ACC- cyanobacteria strains: *Synechocystis* 6803 (ACC-) (#2), *Microcystis* PMC 810 (ACC-) (#3), *Microcystis* PMC 568 (ACC-) (#4). For comparison, the Ca K-edge EXAFS spectrum of *Cyanothece PCC* 7425 (ACC+) (#1) is also shown.

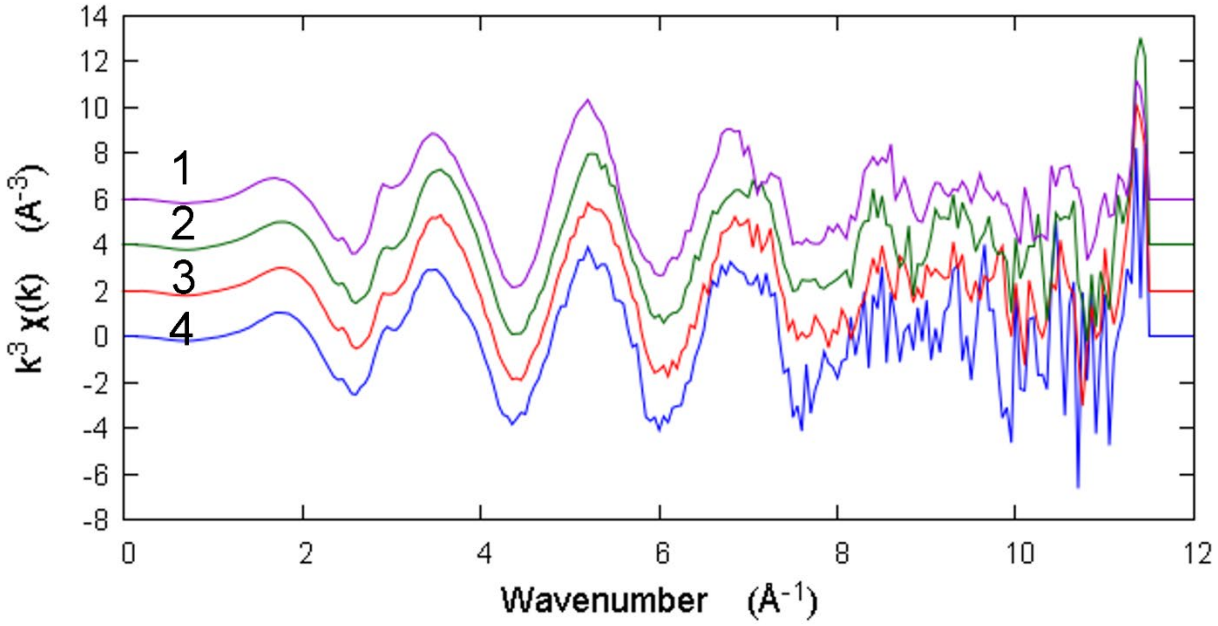

Table S1: Concentrations in solutions used for the synthesis of ACC series with varying a Ca: Mg molar ratio.

	Na_2CO_3 (or K_2CO_3)	$CaCl_2$	$MgCl_2$	Ca	Mg	Ca:Mg
	M	M	M	mol%	mol%	
ACC1*	0.10	0.10	0.9	43.4	56.6	0.8
ACC2*	0.10	0.15	0.85	56.0	44.0	1.3
ACC3*	0.10	0.20	0.8	62.7	37.3	1.7
ACC4*	0.06	0.25	0.75	66.2	33.8	2.0
syn ACC**	0.05	0.045	0.053	71.4	28.6	2.5
ACC5*	0.06	0.30	0.7	78.7	21.3	3.7
ACC6*	0.06	0.40	0.6	86.4	13.6	6.4
ACC7*	0.06	0.50	0.5	88.9	11.1	8.0
ACC8*	0.06	0.45	0.55	89.6	10.4	8.6
*synthesized by mixing Na_2CO_3 with calcium-magnesium solution						
**synthesized by mixing K_2CO_3 with calcium-magnesium solution; Ca: Mg ratio as reported in [4]						

Table S2: Linear combination fitting of derivative XANES spectra of cyanobacteria (ACC+) strains using synthetic ACC and cyanobacteria (ACC-) as fit components. The error on the weight of each component is ~10%.

	Fit components for XANES LCF analyses					
	Synechocystis PCC 6803	ACC*	*Microcystis PMC 810*	*Microcystis PMC 568*	red. chi square	R-factor
Cyanothece PCC 7425 (ACC+)	16	84			5.81E-05	4.28E-03
Synechococcus PCC 6312 (ACC+)	19	81			4.71E-05	3.42E-03
Ca. T.ahousahtiae (ACC+)	23	77			7.23E-05	5.50E-03
Microcystis PMC 827 (ACC+)		70	30		4.51E-05	3.46E-03
Microcystis PMC 831 (ACC+)		59	41		4.48E-05	3.46E-03
Microcystis PMC 827 (ACC+)		67		33	4.62E-05	3.54E-03
Microcystis PMC 831 (ACC+)		55		45	4.69E-05	3.62E-03

*The best fit was obtained with ACC6 (see table S1) with Ca: Mg ratio of 6.4

802 Table S3: Atomic ratios of Mg-P-Ca within carbonate inclusions formed by *Cyanothece* PCC
803 7425 grown in BG-11 medium. The semi-quantitative atomic ratios were calculated using
804 STEM-EDX microanalyses according to [13]

ACC inclusion	Mg	P	Ca	Mg/(Mg+Ca)	P/(P+Ca)
#	atom %	atom %	atom %	atom %	atom %
1	0.2	0	12.98	1.5%	0.0%
2	0.28	0.15	9.82	2.8%	1.5%
3	0.23	0.23	9.44	2.4%	2.4%
4	0.24	0.02	10.29	2.3%	0.2%
5	0.35	0.25	10.32	3.3%	2.4%
6	0.22	0.5	6.13	3.5%	7.5%
7	0.19	0.19	7.94	2.3%	2.3%
8	0.09	0.16	8.8	1.0%	1.8%
9	0.21	0.23	8.51	2.4%	2.6%
10	0.19	0.18	8.99	2.1%	2.0%
11	0.37	0.28	8.25	4.3%	3.3%
12	0.32	0.07	9.14	3.4%	0.8%
13	0.3	0.15	9.18	3.2%	1.6%
14	0.4	0.18	12.48	3.1%	1.4%
15	0.5	0.22	9.32	5.1%	2.3%
16	0.68	0.14	12.61	5.1%	1.1%
17	0.47	0.13	10.15	4.4%	1.3%
18	0.54	0.37	12.07	4.3%	3.0%
19	0.51	0.15	11.8	4.1%	1.3%
20	0.68	0.33	12.34	5.2%	2.6%
21	0.28	0.28	10.25	2.7%	2.7%
22	0.41	0.06	12.29	3.2%	0.5%
23	0.13	0.12	13.32	1.0%	0.9%
24	0.33	0.03	12.83	2.5%	0.2%
25	0.32	0.06	10.4	3.0%	0.6%
26	0.27	0	8.91	2.9%	0.0%
27	0.24	0.12	10.29	2.3%	1.2%
28	0	0	7.75	0.0%	0.0%
29	0	0	10.12	0.0%	0.0%
30	0.01	0.06	9.77	0.1%	0.6%
31	0.14	0	7.7	1.8%	0.0%
32	0	0.09	9.19	0.0%	1.0%
33	0.11	0	8.73	1.2%	0.0%
34	0	0	8.31	0.0%	0.0%
35	0	0	7.47	0.0%	0.0%

36	0	0	9.4	0.0%	0.0%
37	0.24	0.02	12.72	1.9%	0.2%
38	0.3	0.1	10.06	2.9%	1.0%
39	0	0	7.51	0.0%	0.0%
40	0.35	0	9.15	3.7%	0.0%
41	0.48	0.28	8.4	5.4%	3.2%
42	0.69	0.2	9.1	7.0%	2.2%
43	0.16	0.16	5.96	2.6%	2.6%
44	0.26	0.21	7.35	3.4%	2.8%
45	0.18	0.17	9.46	1.9%	1.8%
46	0.48	0.59	11.81	3.9%	4.8%
47	0.34	0.11	8.45	3.9%	1.3%
48	0.28	0.22	8.48	3.2%	2.5%
49	0.26	0	6.52	3.8%	0.0%
50	0.55	0.07	7.09	7.2%	1.0%
51	0.41	0.08	9.16	4.3%	0.9%
52	1.23	1.4	9.05	12.0%	13.4%
53	0.55	0	9.02	5.7%	0.0%
54	0.66	0.25	9.38	6.6%	2.6%
55	0.31	0	6.54	4.5%	0.0%
56	0.42	0.19	7.55	5.3%	2.5%
57	0.37	0.18	12.08	3.0%	1.5%
58	0.28	0.17	9.66	2.8%	1.7%
59	0.58	0.18	9.07	6.0%	1.9%
60	0.47	0.13	9.42	4.8%	1.4%
61	0.28	0.02	10.4	2.6%	0.2%
62	0.23	0.01	7.51	3.0%	0.1%
63	0.19	0.16	7.98	2.3%	2.0%
64	0.32	0.1	8.92	3.5%	1.1%
65	0.43	0.59	8.89	4.6%	6.2%
66	0.26	0.07	10.63	2.4%	0.7%
67	0.29	0.14	8.16	3.4%	1.7%
68	0.19	0.35	6.59	2.8%	5.0%
Average	0.31	0.16	9.40	3.2%	1.7%
Std deviation	0.21	0.20	1.77	2.0%	2.1%

Table S4: The R-factor of the EXAFS fit of *Cyanothece* PCC 7425 upon increasing the Debye-Waller factor of Ca-Ca shell from 0.002 to 0.006. The amplitude reduction factor S_0^2 and ΔE_o were respectively set to 0.88 and 0.41 eV. Text in red shows the parameters changed upon changing the Debye-Waller factor of Ca-Ca shell.

Ca-O shell			Ca-C shell			Ca-Ca shell			
N	R (Å)	σ^2 (Å^2)	N	R (Å)	σ^2 (Å^2)	N	R (Å)	σ^2 (Å^2)	R-factor
3.7 ± 0.2	2.33 ± 0.01	0.002 ± 0.0004	2.8 ± 0.7	3.56 ± 0.02	0.002 ± 0.001	0.5 ± 0.2	3.86 ± 0.02	0.002 ± 0.001	0.0317
4.1 ± 0.2	2.49 ± 0.01	0.002 ± 0.0004							

Ca-O shell			Ca-C shell			Ca-Ca shell			
N	R (Å)	σ^2 (Å^2)	N	R (Å)	σ^2 (Å^2)	N	R (Å)	σ^2 (Å^2)	R-factor
3.7 ± 0.2	2.33 ± 0.01	0.002 ± 0.0004	3.0 ± 0.7	3.56 ± 0.02	0.002 ± 0.001	0.7 ± 0.2	3.86 ± 0.02	**0.004 ± 0.002**	**0.0319**
4.2 ± 0.2	2.49 ± 0.01	0.002 ± 0.0004							

Ca-O shell			Ca-C shell			Ca-Ca shell			
N	R (Å)	σ^2 (Å^2)	N	R (Å)	σ^2 (Å^2)	N	R (Å)	σ^2 (Å^2)	R-factor
3.7 ± 0.2	2.33 ± 0.01	0.002 ± 0.0004	2.9 ± 0.7	3.55 ± 0.02	0.002 ± 0.001	0.8 ± 0.2	3.86 ± 0.02	**0.006 ± 0.003**	**0.0321**
4.2 ± 0.2	2.49 ± 0.01	0.002 ± 0.0004							

References

[1] S. Von Euw *et al.*. "Solid-State Phase Transformation and Self-Assembly of Amorphous Nanoparticles into Higher-Order Mineral Structures." *Journal of the American Chemical Society*. vol. 142. no. 29. pp. 12811–12825. 2020. doi: 10.1021/jacs.0c05591.

[2] N. Koga. Y. Nakagoe. and H. Tanaka. "Crystallization of amorphous calcium carbonate." *Thermochimica Acta*. vol. 318. no. 1. pp. 239–244. Sep. 1998. doi: 10.1016/S0040-6031(98)00348-7.

[3] A. V. Radha. A. Fernandez-Martinez. Y. Hu. Y.-S. Jun. G. A. Waychunas. and A. Navrotsky. "Energetic and structural studies of amorphous Ca1−xMgxCO3·nH2O (0⩽x⩽1)." *Geochimica et Cosmochimica Acta*. vol. 90. pp. 83–95. Aug. 2012. doi: 10.1016/j.gca.2012.04.056.

[4] H. Nebel and M. Epple. "Continuous preparation of calcite. aragonite and vaterite. and of magnesium-substituted amorphous calcium carbonate (Mg-ACC)." *Zeitschrift fur Anorganische und Allgemeine Chemie*. vol. 634. no. 8. pp. 1439–1443. 2008. doi: 10.1002/zaac.200800134.

[5] N. Mehta. J. Gaëtan. P. Giura. T. Azaïs. and K. Benzerara. "Detection of biogenic amorphous calcium carbonate (ACC) formed by bacteria using FTIR spectroscopy." *Spectrochimica Acta Part A: Molecular and Biomolecular Spectroscopy*. vol. 278. p. 121262. Oct. 2022. doi: 10.1016/j.saa.2022.121262.

[6] R. Y. Stanier. J. Deruelles. R. Rippka. M. Herdman. and J. B. Waterbury. "Generic Assignments. Strain Histories and Properties of Pure Cultures of Cyanobacteria." *Microbiology*. vol. 111. no. 1. pp. 1–61. 1979. doi: 10.1099/00221287-111-1-1.

[7] J. Gaëtan *et al.*. "Widespread formation of intracellular calcium carbonates by the bloom-forming cyanobacterium *MICROCYSTIS*." *Environmental Microbiology*. pp. 1462-2920.16322. Dec. 2022. doi: 10.1111/1462-2920.16322.

[8] A.-M. Flank *et al.*. "LUCIA. a microfocus soft XAS beamline." *Nuclear Instruments and Methods in Physics Research Section B: Beam Interactions with Materials and Atoms*. vol. 246. no. 1. pp. 269–274. May 2006. doi: 10.1016/j.nimb.2005.12.007.

[9] D. Vantelon *et al.*. "The LUCIA beamline at SOLEIL." *J Synchrotron Rad*. vol. 23. no. 2. pp. 635–640. Mar. 2016. doi: 10.1107/S1600577516000746.

[10] G. Aquilanti *et al.*. "Operando characterization of batteries using x-ray absorption spectroscopy: advances at the beamline XAFS at synchrotron Elettra." *J. Phys. D: Appl. Phys.*. vol. 50. no. 7. p. 074001. Jan. 2017. doi: 10.1088/1361-6463/aa519a.

[11] B. Ravel and M. Newville. "ATHENA. ARTEMIS. HEPHAESTUS: Data analysis for X-ray absorption spectroscopy using IFEFFIT." in *Journal of Synchrotron Radiation*. Jul. 2005. vol. 12. no. 4. pp. 537–541. doi: 10.1107/S0909049505012719.

[12] J. P. R. De Villiers. "Crystal Structures of Aragonite. Strontianite. and Witherite." *American Mineralogist*. vol. 56. no. 5–6. pp. 758–767. Jun. 1971.

[13] J. Li *et al.*. "Biomineralization Patterns of Intracellular Carbonatogenesis in Cyanobacteria: Molecular Hypotheses." *Minerals*. vol. 6. no. 1. p. 10. 2016. doi: 10.3390/min6010010.